An investigation into the sampling bias of Argo profiling floats in the Southern Ocean

By

TSEI SENAM

SUPERVISORS: SEBASTIAAN SWART (CSIR) AND

BJÖRN BACKEBERG (UCT, OCEANOGRAPHY DPT.)

Department of Biological Sciences
University of Cape Town

Rondebosch, Cape Town

South Africa 7701

August, 2015

Minor dissertation submitted in partial fulfillment of the requirements for the Degree of Master of Science in Applied Marine Science

The financial assistance of the National Research Foundation (NRF) towards this research is hereby acknowledged. Opinions expressed and conclusions arrived at, are those of the author and are not necessarily to be attributed to the NRF.

ABSTRACT

Numerous Argo floats (approximately 3800 floats) have been deployed in the world's oceans to gather hydrographic and biogeochemical data from the upper 2000 m. However, limited research has been done on the spatial and temporal distribution and potential sampling bias of Argo profiling floats brought on by the effects of bathymetric steering of currents, as well as oceanic features, such as meanders and eddies, that affect their distribution over the global ocean. This study investigates the sampling distribution of profiling floats and assesses the mechanisms that impact their trajectories and distribution in the Atlantic sector of the Southern Ocean. The study reveals that Argo floats are influenced and steered towards frontal jets, which in turn are steered by the underlying bathymetry. Argo floats have a 30 % higher probability of sampling regions where depths range from 4000 - 5000 m, rather than shallow regions of the oceans. Using bootstrapping, this result was shown to be statistically significant at the 95 % confidence interval. The sampling bias is associated with floats becoming entrained into deep reaching frontal jets that occur in the Southern Ocean and dominate the deeper waters. This is shown by analyzing the Argo float positions in relation to mean geostrophic currents which shows that there is a 40 % higher probability (statistically significant at the 95 % confidence level) of finding Argo floats in regions where geostrophic currents range from 0.1 - 0.22 $m.s^{-1}$ even though the majority of surface currents in the Southern Ocean are found below 0.05 $m.s^{-1}$. This indicates a non-uniform distribution of Argo floats in the Southern Ocean, which leads to a spatial sampling bias in the float data. This has implications for how we characterize the oceanography or understand the distribution and variability of oceanographic processes and its relation to climate.

Table of contents

Contents	Pages
1. Introduction	**8**
2. Data and Methods	**14**
2.1. Study Region	**14**
2.2. Argo float data	**15**
2.3. Bathymetry	**16**
2.4. Altimetry-derived surface geostrophic current velocities	**17**
2.5. Assessing the relationship between float distribution with bathymetry and surface geostrophic velocities	**17**
3. Results	**20**
3.1. Argo floats and bathymetry	**20**
3.2. Argo floats and altimetry-derived surface geostrophic current velocities	**25**
4. Discussion	**30**
4.1. Argo floats and relation to bathymetry	**30**
4.2. Argo floats and relation to altimetry-derived surface geostrophic current velocities	**33**
5. Summary and challenges	**35**
Acknowledgements	**38**
References	**40**

List of figures

Figure 1: The frequency of occurrence of front positions at grid points where the fronts were observed at least 0.4% of the time. Colour range varies between 0.4 and 10 %. Only the middle branches of the Sub-Antarctic Front and Polar Front and the northern branch of the South Antarctic Circumpolar Current Front and the Southern Boundary are shown. The mean position of each frontal branch, derived by contouring the mean SSH field, is indicated by the central thick solid line. The 2000 m isobaths are indicated by light blue lines (taken from Sokolov and Rintoul, 2009b).

Figure 2: The study region (in black) showing the main ACC fronts (in magenta) superimposed on the bathymetry. The northernmost front is the SAF, followed by the PF, the sACCf and SBdy respectively. The major topographic features in the region are: the Agulhas Ridge (1), the Meteor Rise (2), the Southwestern Indian Ridge (3), Crozet Island and Del Caño Rise (4), the Conrad Rise (5) and the Agulhas Plateau (6). The GoodHope Line (GHL) is shown by the red dashed line.

Figure 3: The distribution of co-located Argo profiling floats and bathymetry binned in 200 m depth intervals in terms of percentage occurrences. The bins sum up to 100 %.

Figure 4: The distribution of bathymetry data ($topo_{total}$) of the Southern Ocean south of Africa in terms of percentage occurrences. The bathymetry is binned in 200 depth intervals. The bins sum up to 100 %.

Figure 5: The ratio of the percentages of the co-located Argo profiling floats instances in relation to the bathymetry — $topo_{floats}$ (as depicted in Figure 3) and the percentage distribution of the bathymetry of the focus area — $topo_{total}$ (as depicted in Figure 4). This ratio provides a quantitative evaluation of the expected presence of floats within certain depth bins normalized by the bathymetry distribution present in the region of study. A bias is identified where the ratio $B_{topo} > 1$. A bias is statistically significant when the limits of 95 % confidence interval lie above 1. The green and the magenta lines represent the lower and the upper limits (2.5 % and 97.5 %) of the confidence interval respectively.

Figure 6: Schematic representation of trajectories of a portion of Argo profiling floats deployed at the GoodHope Line overlaid on the bathymetry. The floats can qualitatively be seen to be steered by bathymetry – i.e. mostly avoiding shallower regions. The dashed circles represent regions of convergence of floats into individual fronts: magenta (SAF), red (PF), brown (sACCf) and blue (SBdy). The black contours describe the mean location of the main ACC fronts from north to south: SAF, PF, sACCf and SBdy.

Figure 7: 3D illustration of the steering of three chosen Argo floats by the underlying bathymetry. The trajectories of the floats are represented by black, blue and magenta curves.

Figure 8: The percentage distribution of co-located Argo profiling floats in relation to the surface geostrophic velocities (binned in 0.02 $m.s^{-1}$ intervals). Each bin represents a percentage. The bins sum up to 100 %.

Figure 9: The distribution of the mean surface geostrophic current velocities (vel_{total}) of the focus region in terms of percentage occurrences. The velocities were binned in 0.02 $m.s^{-1}$ intervals**.** The bins sum up to 100 %.

Figure 10: The ratio of the percentages of the co-located Argo profiling floats instances (vel_{floats}) in relation to the surface velocity (as depicted in Figure 8) and the distribution of the mean surface velocity (vel_{total}) (as depicted in Figure 9) of the Southern Ocean south of Africa. This ratio, $B_{vel,}$ provides a quantitative evaluation of the expected presence of floats within certain velocity bins normalized by the velocity distribution present in the region of study. A bias is identified where the ratio, $B_{vel} > 1$ and is statistically significant when the limits of 95 % confidence interval lie above 1.The green and the magenta lines represent the lower and the upper (2.5 % and 97.5 %) limits of the confidence interval respectively.

Figure 11: Locations of floats that have positive bias in the velocity bins between 0.1 - 0.22 $m.s^{-1}$ (yellow dots) as depicted in Figure 10. The floats are overlaid on to the mean surface geostrophic velocities. The red contours describe the mean location of the main ACC fronts from north to south: SAF, PF, sACCf and SBdy.

Figure 12: A conceptual diagram describing the Argo floats sampling sequence and the deep reaching fronts of the ACC. The Argo floats drift for 10 days at the parking depth (PD). The floats at the GoodHope Line (GHL) are normally distributed evenly in uniform fashion. Downstream, these floats aggregate as they are entrained into the fronts after deployment. The cores of the fronts are seen to be deep reaching and therefore are impacted by underlying topography resulting in meandering and spatial variability in the distribution of the fronts.

1. Introduction

The most notable feature of the Southern Ocean is the Antarctic Circumpolar Current (ACC). The ACC is an eastward flow that extends around the globe and it is driven by the westerly winds found between 45º - 55º S (Orsi et al., 1995). The absence of a continental barrier in the latitude band of the Drake Passage allows the ACC to flow uninterrupted around the entire Southern Ocean, thereby connecting the South Atlantic, South Indian and South Pacific Oceans. The ability of the ACC to flow uninterrupted between ocean basins permits a global overturning to exist (Rintoul et al., 2001; Talley et al., 2011). This overturning circulation transports heat, fresh water and other properties, which influence the global climate (Gordon, 1986; Rintoul et al., 2001; Sokolov and Rintoul, 2007; Sokolov and Rintoul, 2009a). In addition, the inter-basin exchanges, facilitated by the ACC, allow for heat and other water properties to be carried around the globe and to affect remote climatic conditions (Gille, 2008).

Sokolov and Rintoul (2009a) explained that the ACC is made up of multiple fronts: the Sub-Antarctic Front (SAF), the Polar Front (PF), the Southern ACC Front (sACCf) and the Southern Boundary (SBdy). These fronts are robust and persistent features in time and space (Orsi et al., 1995; Rintoul et al., 2001; Sokolov and Rintoul, 2002; 2007; 2009b). Sokolov and Rintoul (2007) explained that many of the ACC main fronts consist of multiple branches or filaments, which merge and diverge along the circumpolar path.

The ACC fronts are deep reaching jets and are aligned along particular streamlines of constant dynamic heights throughout the circumpolar path of the current (Deacon, 1937; Nowlin and Clifford, 1982; Sievers and Nowlin, 1984; Orsi et al., 1995; Belkin and Gordon, 1996; Sokolov

and Rintoul, 2009a, Swart et al., 2010). Sokolov and Rintoul (2009b) further described the frontal jets of the ACC by fitting sea surface heights (SSH) to the mean dynamic topographic maps and calculating the frequency of occurrence of the frontal positions (Figure 1). Their method agrees well with water mass properties (classical method) used by Orsi et al. (1995) to define the ACC fronts. In addition to this, previous studies had observed large changes in the SSH of the Southern Ocean (Willis et al., 2004; Lombard et al., 2005; Morrow et al., 2008). SSH contours of constant dynamic heights are associated with particular ACC fronts. Hence changes in SSH may reflect shifts in the position of the ACC fronts in time and space (Figure 1). Most of the variability and changes observed in some areas are associated with the interaction of the fronts with the complex underlying bathymetry (Gille and Kelly, 1996; Swart et al., 2008; Sokolov and Rintoul, 2009a; Graham et al., 2012). For example, the northern branch of the PF is deflected northwards towards the equator near the Kerguelen Plateau (Graham et al., 2012). In order to conserve potential vorticity in barotropic currents, such as the ACC, their trajectories are diverted by the ocean topography. As the depth decreases, due to the presence of a shallow topographic barrier, the relative vorticity and Coriolis parameter must also decrease so that potential vorticity is conserved. Consequently, ACC fronts are deflected northwards over shallow topographic features. In contrast, ACC fronts are occasionally fixed to a particular position and cannot shift. This is known as topographic blocking, where the bathymetry inhibits the movement of fronts in the Southern Ocean (Moore et al., 1999; Gille, 2003; Sokolov and Rintoul, 2007).

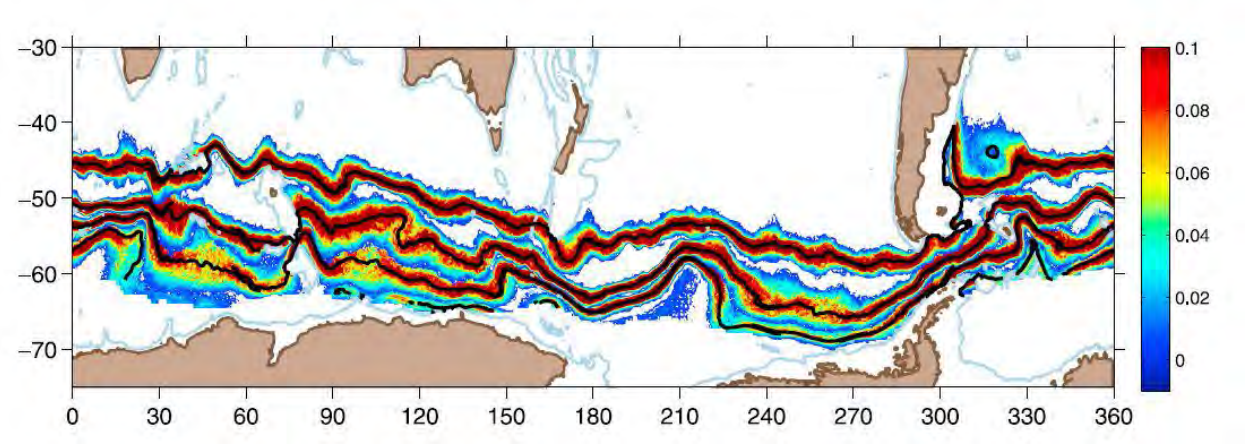

Figure 1: The frequency of occurrence of front positions at grid points where the fronts were observed at least 0.4% of the time. Colour range varies between 0.4 and 10 %. Only the middle branches of the Sub-Antarctic Front and Polar Front and the northern branch of the South Antarctic Circumpolar Current Front and the Southern Boundary are shown. The mean position of each frontal branch, derived by contouring the mean SSH field, is indicated by the central thick solid line. The 2000 m isobaths are indicated by light blue lines (taken from Sokolov and Rintoul, 2009b)

South of Africa, the ACC is affected by the oceanographic systems occurring north and south of its borders (Swart et al., 2008), namely the Agulhas Current system and the Weddell Gyre. The Agulhas Retroflection determines the latitudinal extent of the northernmost front of the ACC south of Africa (Belkin and Gordon, 1996; Swart et al., 2008). Moreover, Park et al. (2001) divided the oceanic region between the African and Antarctic continents into three sectors: the subtropical domain (40º - 42˚ S), the core of the ACC (between 40º - 42˚ S and 55º - 57˚ S) and the eastern part of the Weddell Sea gyre to the south (Gladyshev et al., 2008). However, Swart et al. (2008) explain that the SAF has a distinct core jet at 44º S and two additional small jets at 43º S and 44.5º S. They further explain that the PF has three individual transport jets. The three jets are found at 50.8º S (most prevalent), at 49º S and at 48º S (smallest). The sACCf contains two

transport jets that lie at 51.5° S and 52.5° S, respectively. The SBdy is characterized by a small jet found at 55.5° S. Despite its important role in connecting oceanic basins, the ACC south of South Africa has been less studied than its two counterparts south of South America and south of Australia.

The Global Atmospheric Research Program (GARP) provided the scientific community with an opportunity to examine the circumpolar nature of fronts and zones in the Southern Ocean (Hofman, 1985). In the First GARP Experiment (FGGE), surface drifters were deployed to understand the structure of the ACC. This experiment revealed that the surface drifting buoys tended to accumulate in zones of strong currents identified as the fronts in the Southern Ocean, suggesting that the surface drifters were entrained into frontal zones of the ACC (Hofman, 1985). The distribution of the surface drifters created the impression that the circulation of the ACC has a banded structure (Hofman, 1985). This experiment preceded the era of Argo profiling floats and gliders.

Argo profiling floats are lagrangian autonomous profiling platforms that drift with the deep currents in the ocean (Ollitraut and Rannou, 2012). They have enabled continuous and real-time subsurface observations of the global ocean over the past two decades (Ollitraut and Rannou, 2012). Argo floats provide the means to collect vast amounts of hydrographic data from remote and inaccessible regions, such as the Southern Ocean. Argo profiling floats, in their most common mode, gather temperature, salinity and pressure data from the upper 2000 m of the ocean every 10 days and additionally provide estimates of the deep ocean currents (Ollitraut and

Rannou, 2012). These platforms are complementary to remotely sensed satellite observations of the surface ocean because they provide subsurface information on the state of the ocean.

Although Argo profiling floats have contributed to successes in sampling vast and remote areas of the ocean, it is also important to determine whether the quantitative descriptions of these oceans by these Argo profiling floats represent the full regional scale perspective of the ocean. The distributions of fronts and eddies characterizing the Southern Ocean show a spatial distribution influenced by topographic steering (e.g. Swart et al., 2008; Sokolov and Rintoul, 2009a; Graham et al., 2012). These features (fronts and eddies) are hypothesized to entrain the Argo floats into their cores due to convergent mechanisms, which may introduce a spatial bias or error in the distribution of Argo profiling floats. As a result, floats may be sampling only part of the dynamics and related variability associated with the Southern Ocean, which affects the quantitative understanding of the processes and dynamics of the Southern Ocean.

In light of the potential spatial bias in distribution of Argo profiling floats, this study aims to address the following key questions:

1. What is the spatial distribution of the Argo profiling floats in the Southern Ocean south of Africa?
2. Is the spatial distribution of the Argo profiling floats influenced by the bathymetry or by the surface geostrophic velocities in the Southern Ocean?

The dissertation is structured as follows: Section 2 describes the data and methods. Section 3 presents the results in the relation to the bathymetry and the altimetry-derived surface

geostrophic current velocities. Section 4 discusses the results and figures presented in Section 3. Finally, in Section 5, a conclusion is made in relation to the research questions introduced in Section 1.

2. Data and Methods

2.1. Study Region

This study focuses on the African section of the Southern Ocean, in particular the region of the GoodHope monitoring Line (Ansorge et al., 2004; Swart et al., 2008). This region is a meeting point of the eastward flowing ACC and the southwestward flowing Agulhas Current (Bryden et al., 2005; Lutjeharms, 2006; Swart et al., 2008). The data used in this study come from the region between 0º - 50º E and 40º - 60º S (Figure 2). The study area is limited to south of Africa in order to investigate the trajectory of Argo floats deployed annually at the GoodHope Line by research ships and ships of opportunity. In a future study, the domain of this study could be expanded to the entire Southern Ocean.

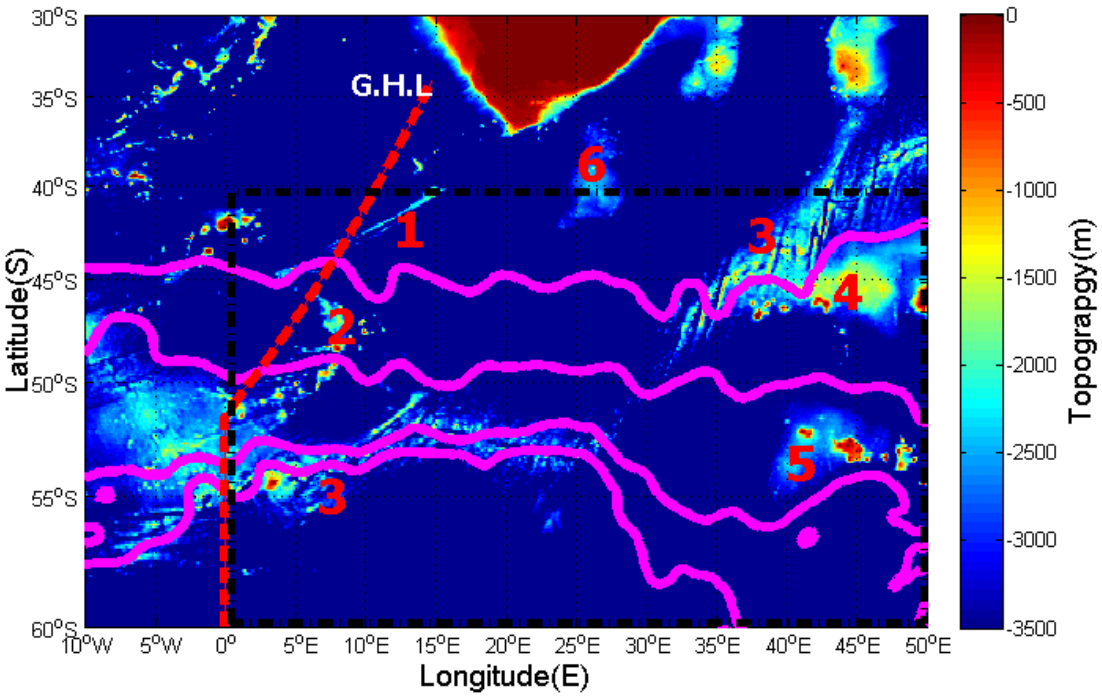

Figure 2: The study region (in black) showing the main ACC fronts (in magenta) superimposed on the bathymetry. The northernmost front is the SAF, followed by the PF, the sACCf and SBdy respectively. The major topographic features in the region are: the Agulhas Ridge (1), the Meteor Rise (2), the Southwestern Indian Ridge (3), Crozet Island and Del Caño Rise (4), the Conrad Rise (5) and the Agulhas Plateau (6). The GoodHope Line (GHL) is shown by the red dashed line.

2.2. Argo float data

Argo float metadata files were used in this study. The data were downloaded from the Global Data Assembly Centre (GDAC, see also Argo, 2000).The dataset is a compilation of Argo float data from the Atlantic Oceanographic and Meteorological Laboratory (AOML, USA), Coriolis (France) and Japan Meteorological Agency (JMA, Japan). The metadata files contain the following information: float characteristics, such as the sensor features, including the pressure gauge model with its calibration formula and coefficients, deployment date and position, surfacing locations, description of the float mission including the duration of the sampling cycle,

parking depth pressure and the deepest pressure (Ollitraut and Rannou, 2012). In this study, only the longitude and latitude positions, launch date and float serial numbers are used. These variables help to identify the floats and obtain their positions with respect to the bathymetry and surface geostrophic current velocity maps. The region of data collection means that primarily Argo profiling floats deployed from the GoodHope Line are used in this study. The metadata files used cover a 17 year period (1997 - 2014) and a total of 167 floats were considered in this study.

2.3. Bathymetry

ETOPO2 is a gridded topography dataset with a spatial resolution of 2-minutes. It is an integration of numerous regional and global data sets and was downloaded from the US National Geophysical Data Center (NGDC). ETOPO2 is based on estimated sea floor features derived from sea surface altimetry measurements from satellites. The sea surface mimics the bumps and dips of the underlying ocean floor. In addition, these bumps and dips are acted upon by gravity of the underlying bathymetry. The gravitational attraction, therefore, creates variations or deflections in the sea surface height. The deflections, though small, are measured from space and converted into gravity. The ETOPO2 dataset was created by exploiting the correlation of bathymetry and gravity (Sandwell, 1990). More information on how this dataset is created can be found in Sandwell and Zhang (1989) and Sandwell and Smith (1997). Only the bathymetry between 40˚ S and 60˚ S (focus region) was considered in this study since the topography over features to the north and over land introduces biases in our statistical calculations of the relationship between floats and bathymetry.

2.4. Altimetry-derived surface geostrophic current velocities

Surface geostrophic current observations were obtained from the Ssalto/Duacs multi-mission altimeter delayed time product from CLS/AVISO, which includes data from four different satellites (T/P, Jason-1, ERS-1/2 and Envisat altimeters). The product contains gridded sea level anomaly data above the mean dynamic topography (Rio et al., 2011), and these data are used to compute geostrophic velocities. The absolute dynamic topography (ADT) is the sum of the sea level anomaly (SLA) measured by the satellite altimeters and the mean dynamic topography (MDT). The MDT is a combined product using *in situ* data, altimetry data and the EIGEN-GRACE 03S geoid. The geostrophic velocity product is gridded to a 1/4° Cartesian grid. For more details on the mapping techniques and error estimation used to generate these data, refer to Le Traon et al. (1998), Le Traon et al. (2001) and Rio et al. (2011).

2.5. Assessing the relationship between float distribution with bathymetry and surface geostrophic velocities

The positions of the Argo profiling floats were co-located in space to the ETOPO2 bathymetry in order to get a value of the underlying bathymetry for each float location in the dataset. To do this, the gridded bathymetry data were linearly interpolated to each longitude and latitude position of every Argo profiling float within the dataset. The bathymetry value at each float location was then binned into 200 m depth intervals between 0 - 6000 m to assess the number of float locations found in each 200 m depth interval of the bathymetry. The percentages of float locations found in each bathymetry bin were then calculated by dividing this by the total number of float positions, which is termed $topo_{float}$.

In order to assess the spatial distribution of the overall regional bathymetry in the study region, the ETOPO2 bathymetry was binned into 200 m depth intervals between 0 to 6000 m depth to estimate the percentage prevalence of the underlying bathymetry at each depth interval, which is termed $topo_{total}$.

In order to understand if the float to bathymetry distribution was a function of the general distribution of the bathymetry or not, the following was undertaken: the percentage of floats found within each depth bin ($topo_{float}$) was divided by the overall binned distribution of the bathymetry ($topo_{total}$). This resulted in a ratio B_{topo} ($topo_{float}$:$topo_{total}$) to identify potential biases between the distribution of floats and the underlying bathymetry (i.e. to assess if floats are found in particular areas of ocean bottom depth).

In order to test whether the identified biases are statically significant, the bootstrap method was applied to calculate the lower and upper limits of the confidence interval. In doing so, the co-located floats and bathymetry ($topo_{float}$) were re-sampled 1000 times to generate new data points to determine the confidence level. The re-sampled data was divided by the bathymetry ($topo_{total}$) to obtain the new ratio. This new ratio was re-arranged from the lowest to the highest to select the lower (2.5 %) and upper (97.5 %) limits of the confidence interval in each 200 m depth interval. The lower and upper limits of the confidence interval were plotted over the ratio B_{topo} ($topo_{float}$:$topo_{total}$) (Figure 5). The resultant biases were statistically significant when both the lower and upper limits of 95 % confidence were larger than 1. However, the biases are not statistically significant when 1 lay between the confidence interval limits.

The same approach was used to assess the float distribution in relation to the mean altimetry-derived surface geostrophic currents in the study region. The geostrophic velocities were binned into 0.02 $m.s^{-1}$ intervals, ranging from 0 - 0.5 $m.s^{-1}$. In this case, the percentage of float locations found in each surface velocity bin was calculated by dividing this by the total number of float positions to derive vel_{float}. The spatial distribution of the overall regional velocities in the study region is termed vel_{total}. Again, a ratio (B_{vel}) was found between these two parameters (vel_{float}:vel_{total}) to identify potential biases in the distribution of floats in relation to the mean surface velocities of the region (i.e. to assess if floats are found in particular areas of higher or lower surface velocities). To test whether the identified biases were statically significant at 95 % confidence interval, the bootstrap method was applied to calculate the lower and upper limits of the confidence interval in the same way as was done for the bathymetry. The co-located floats and mean surface velocities (vel_{float}) were re-sampled 1000 times to generate new data points. This was therefore divided by the mean surface velocity (vel_{total}). This new ratio was re-arranged from the lowest to the highest value to select the lower (2.5 %) and upper (97.5 %) limits of the confidence interval in each 0.02 ms^{-1} velocity bin interval. The lower and upper limits of the confidence interval were plotted over the ratio B_{vel} (vel_{float}:vel_{total}) (Figure 10). The biases were statistically significant when both the lower and upper limits of 95 % confidence was larger than 1.

3. Results

3.1. Argo floats and bathymetry

The co-location of floats with the underlying bathymetry ($topo_{float}$, Figure 3), conducted to examine the distribution of the Argo floats in relation to the bathymetry in the study region, revealed that 67 % of the floats (112 out of 167 floats) were located in the deep ocean between 4000 to 5400 m. Depths ranging from 2400 to 3600 m contained 20 % of the Argo floats, 2.4 % were found between 5600 and 6000 m and 3.3 % of the floats were found in ocean depths ranging from 0 to 2000 m. In summary, less than 6 % of the Argo profiling floats were found in shallow areas and at very deep depths; the majority of the floats were found at depths ranging from 4000 to 5400 m.

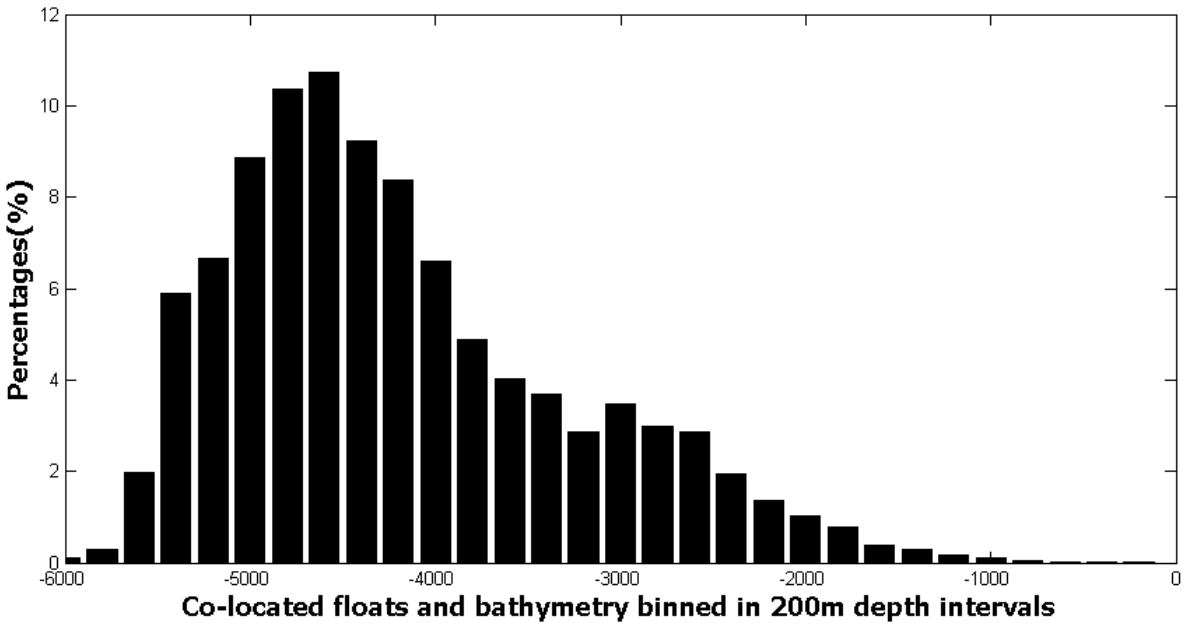

Figure 3: The distribution of co-located Argo profiling floats and bathymetry binned in 200 m depth intervals in terms of percentage occurrences. The bins sum up to 100 %.

The percentage distribution of bathymetry data binned into 200 m depth intervals ($topo_{total}$, Figure 4), conducted to compare the distribution of the depths that floats occupy versus the overall distribution of the bathymetry, showed that 65 % of the study area had depths ranging from 4000 to 5400 m, while 21.6 % of ocean depth south of Africa ranged from 2400 to 3600 m. The 0 to 2000 m depth range covered approximately 3.7 % of the study domain, and ocean depths greater than 5800 m covered less than 3 % of the domain.

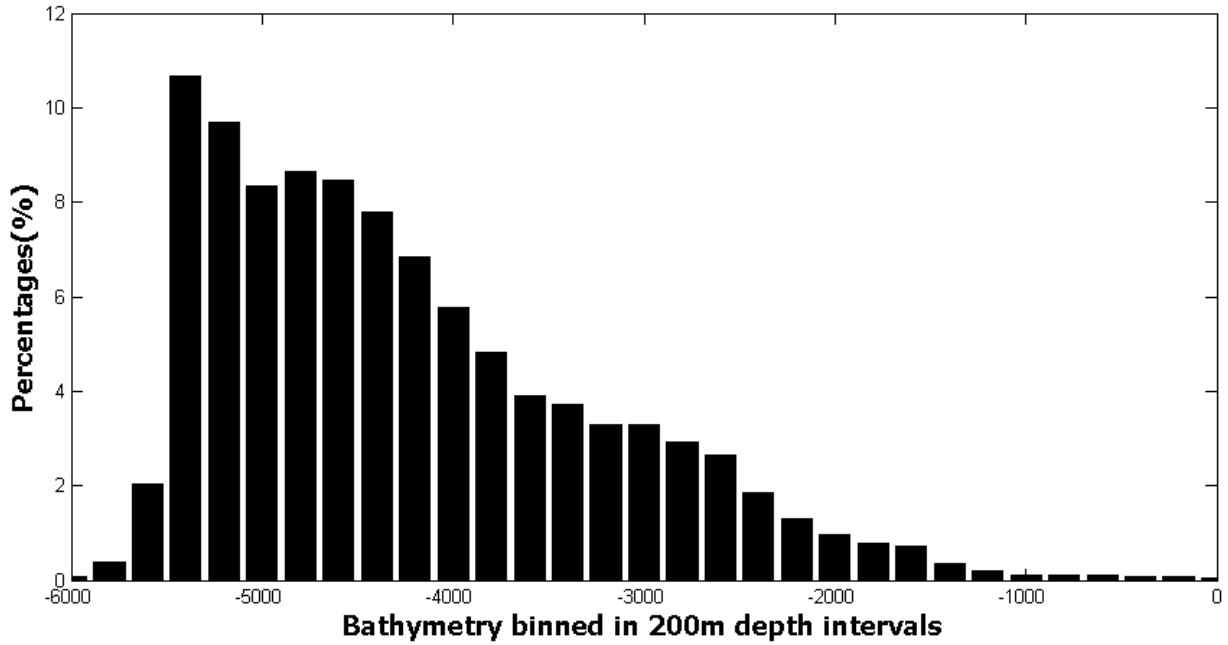

Figure 4: The distribution of bathymetry data ($topo_{total}$) of the Southern Ocean south of Africa in terms of percentage occurrences. The bathymetry is binned in 200 depth intervals. The bins sum up to 100 %.

The ratio of the above percentages B_{topo} ($topo_{float}$ / $topo_{total}$) calculated to estimate the potential spatial sampling bias of the Argo profiling floats, effectively showed that only a depth range (where $B_{topo} > 1$) was statistically significant at 95 % confidence interval. This was in regions where the ocean depth ranged from 4000 m to 5000 m (Figure 5). The identified bias ranged from 1.1 to 1.25 (4000 - 5000 m). This suggests that there was a 10 - 30 % higher probability of

finding floats within depths ranging from 4000 m to 5000 m with a small hiatus when B_{topo} was slightly less than 1 (8.9 - 0.98) in a depth range of 3400 - 3800 m. However, there was a low percentage probability ($B_{topo} < 1$) in shallow regions (0 - 1800 m) and in some deep regions (5200 - 5800 m). Furthermore, Figure 5 indicated that floats tended to be uniformly distributed in 2000 - 3000 m depth range at 95 % confidence interval.

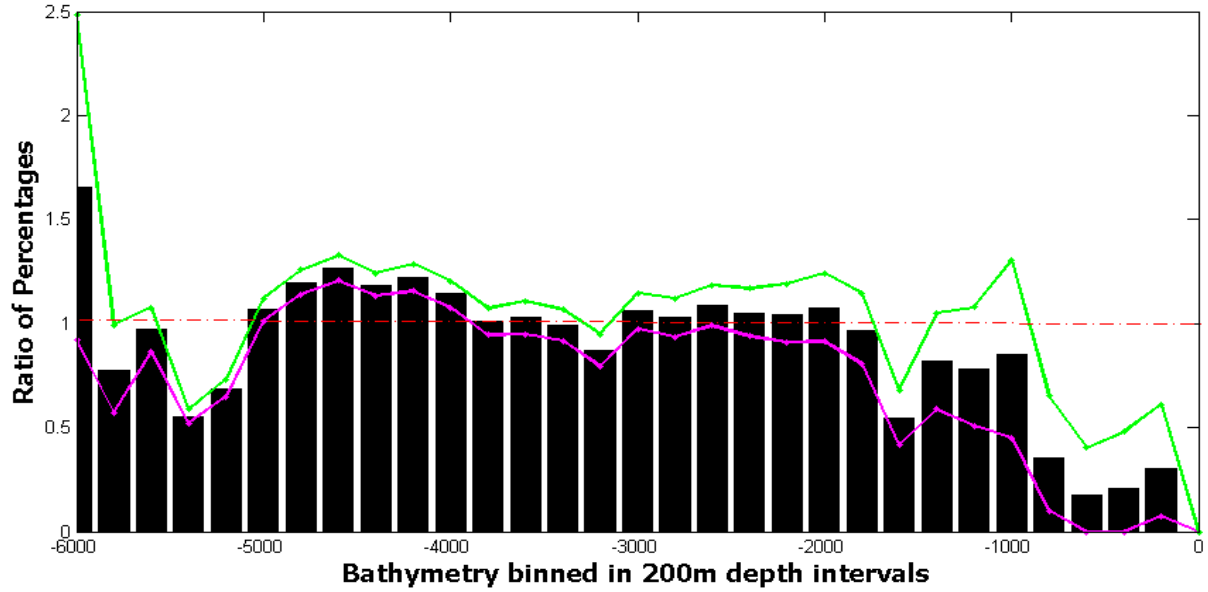

Figure 5: The ratio of the percentages of the co-located Argo profiling floats instances in relation to the bathymetry — $topo_{floats}$ (as depicted in Figure 3) and the percentage distribution of the bathymetry of the focus area — $topo_{total}$ (as depicted in Figure 4). This ratio provides a quantitative evaluation of the expected presence of floats within certain depth bins normalized by the bathymetry distribution present in the region of study. A bias is identified where the ratio $B_{topo} > 1$. A bias is statistically significant when the limits of 95 % confidence interval lie above 1. The green and the magenta lines represent the lower and the upper limits (2.5 % and 97.5 %) of the confidence interval respectively.

The trajectories of the Argo profiling floats deployed along the GoodHope Line were plotted over the underlying bathymetry and the ACC fronts (black contours) to highlight the relationship between the Argo floats and the bathymetry (Figure 6). These Argo floats illustrated qualitatively the overall topographic steering by the underlying bathymetry. A zone of convergence of trajectories of Argo floats was observed in the Agulhas Basin at latitudes of the SAF. Further to the east (near the Southwestern Indian Ridge), similar zones of convergence were observed. These zones may be associated with branches of the SAF. Additional converging zones of Argo profiling floats were identified at higher latitudes (Figure 6) in the latitudinal bands of the PF, sACCf and SBdy. In summary, the results presented in Figure 6 suggest that the trajectories of the Argo profiling floats closely match the pathways of the ACC fronts.

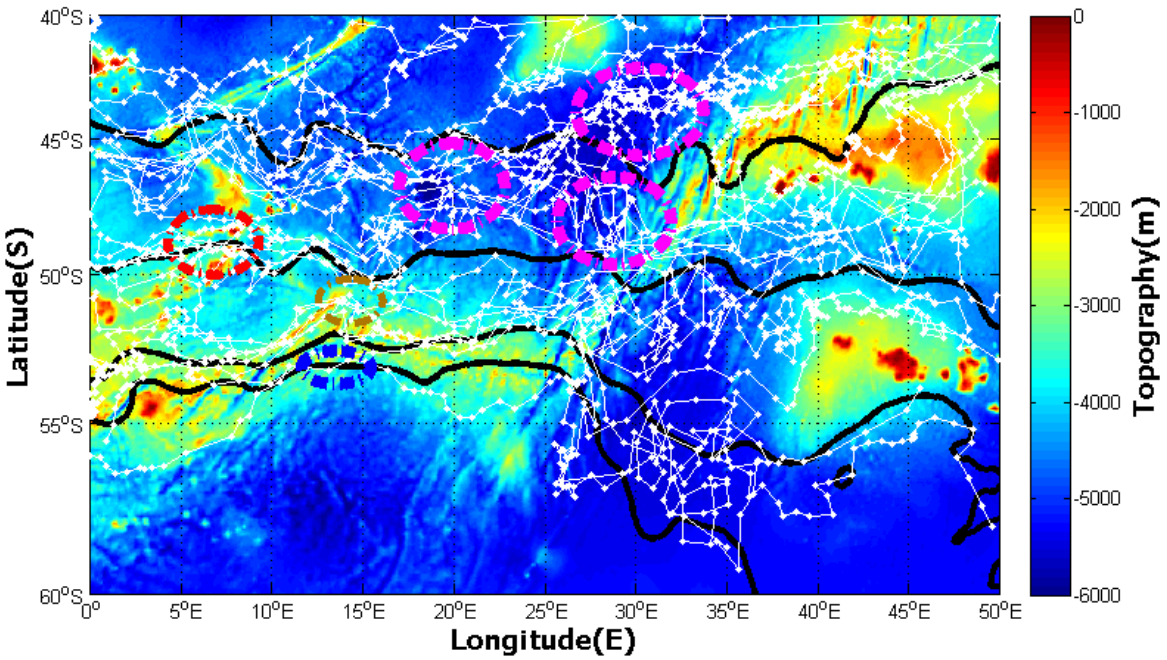

Figure 6: Schematic representation of trajectories of a portion of Argo profiling floats deployed at the GoodHope Line overlaid on the bathymetry. The floats can qualitatively be seen to be steered by bathymetry – i.e. mostly avoiding shallower regions. The dashed circles represent regions of convergence of floats into individual fronts: magenta (SAF), red (PF), brown (sACCf) and blue (SBdy). The black contours describe the mean location of the main ACC fronts from north to south: SAF, PF, sACCf and SBdy.

Figure 7 highlights three Argo profiling float trajectories being influenced by topographic features of the Southern Ocean. The three chosen trajectories tend to remain in waters deeper than 3500 m, suggesting that they are entrained into circulation features of the ACC that are topographically steered.

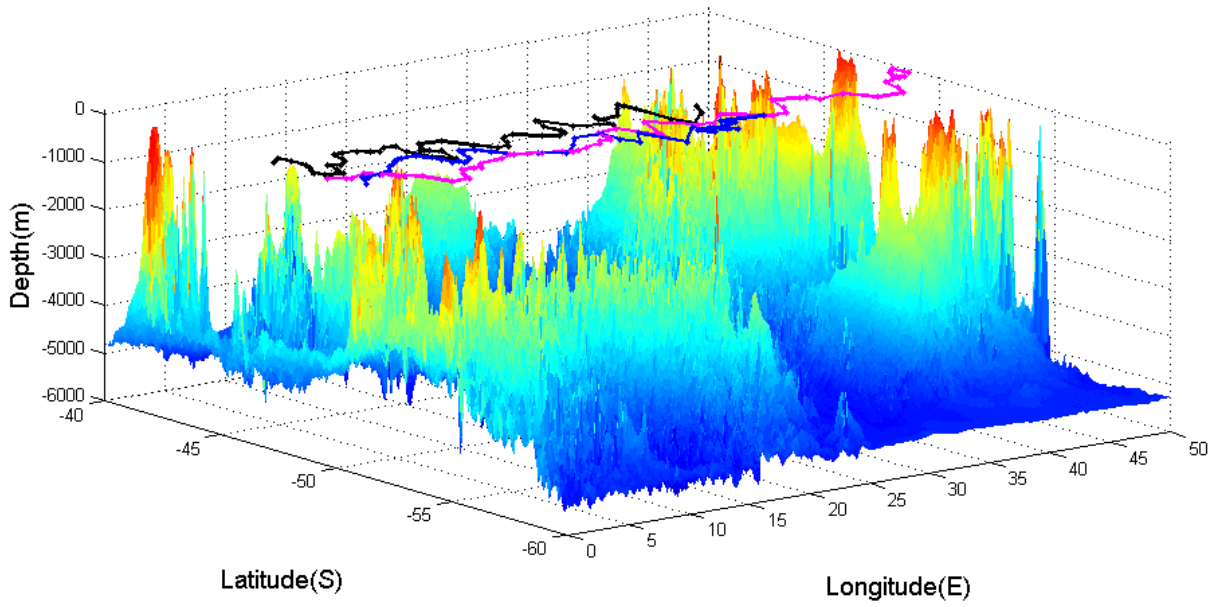

Figure 7: 3D illustration of the steering of three chosen Argo floats by the underlying bathymetry. The trajectories of the floats are represented by black, blue and magenta curves.

3.2. Argo floats and altimetry-derived surface geostrophic current velocities

The interpolation of Argo float positions on to the mean satellite-derived surface geostrophic current velocities (vel_{float}) was conducted to examine the relationship between the spatial distribution of Argo float positions and areas of enhanced surface flow (frequently associated with the fronts of the ACC in detail) (Figure 8). This revealed that 73.2 % (123 out of 167 floats) in the region were found where the mean surface geostrophic current velocities ranged from 0.04 to 0.16 $m.s^{-1}$. Approximately, 7 % of the total floats were found where the mean surface geostrophic velocities ranged from 0.24 - 0.5 $m.s^{-1}$.

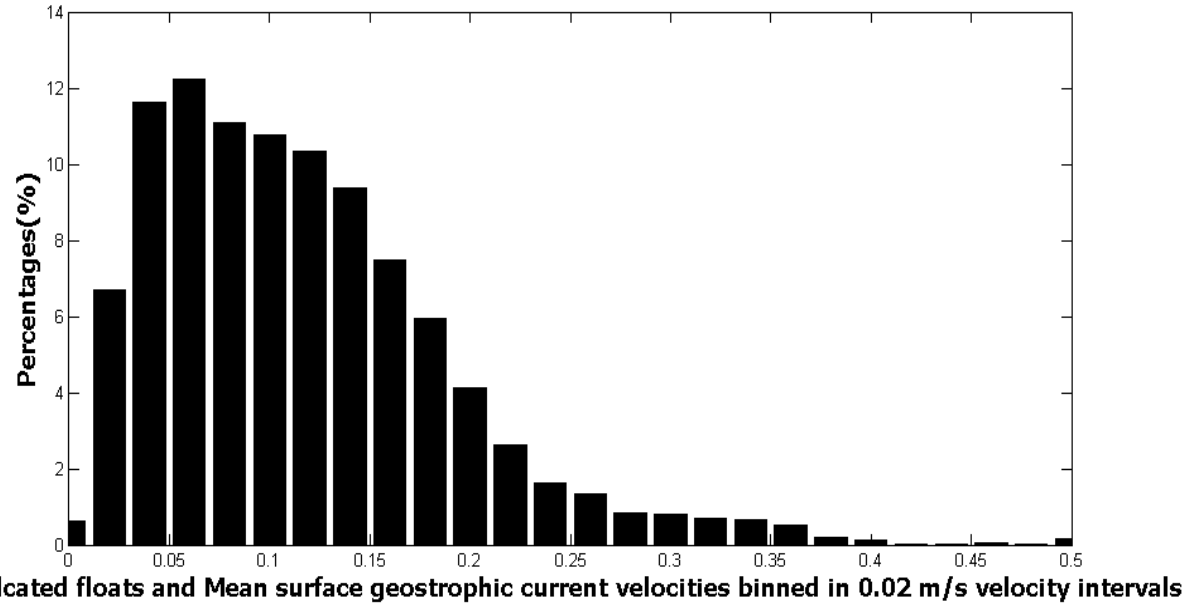

Figure 8: The percentage distribution of co-located Argo profiling floats in relation to the surface geostrophic velocities (binned in 0.02 m.s^{-1} intervals). Each bin represents a percentage. The bins sum up to 100 %.

The percentage distribution of the mean surface geostrophic current velocities (binned in 0.02 m.s^{-1} velocity intervals) was calculated to obtain the total distribution of mean surface geostrophic current velocities in the study region and showed that 62 % of the surface geostrophic velocities in the region ranged from 0.02 - 0.1 m.s^{-1}, and 33 % of the region had a mean surface velocity ranging from 0.12 - 0.5 m.s^{-1} (Figure 9).

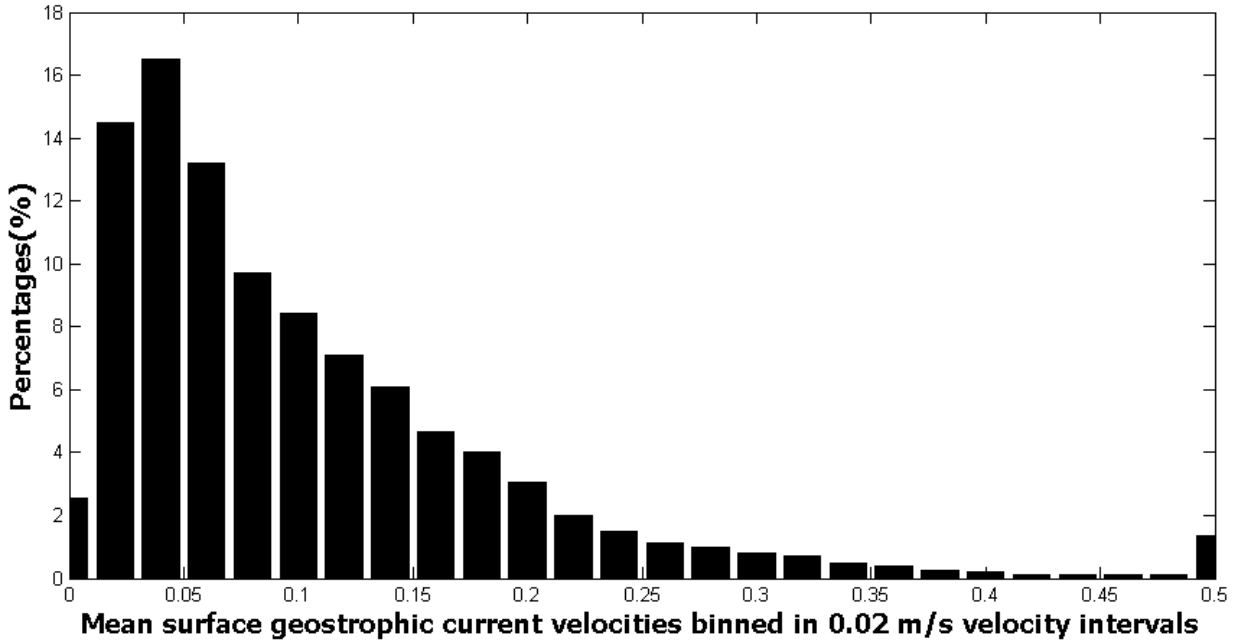

Figure 9: The distribution of the mean surface geostrophic current velocities (vel_{total}) of the focus region in terms of percentage occurrences. The velocities were binned in 0.02 $m.s^{-1}$ intervals. The bins sum up to 100 %.

The ratio of the percentages of floats interpolated to mean surface geostrophic velocities (vel_{floats}) and the percentages of the total distribution of altimetry-derived surface geostrophic current velocities (vel_{total}) ($B_{vel} = vel_{floats} / vel_{total}$), conducted to test for a potential bias in the spatial distribution of Argo floats in relation to the mean surface geostrophic current velocities, highlighted that a bias ($B_{vel} > 1$) in 0.1 - 0.22 $m.s^{-1}$ velocity range was statistically significant at 95 % confidence interval. However, the bias identified at the 0.34 - 0.36 $m.s^{-1}$ velocity range is not statistically significant at the 95 % confidence interval. Figure 10 further suggests that there was up to 40 % higher percentage probability of finding Argo floats where current velocities ranged from 0.1 - 0.22 $m.s^{-1}$. A small hiatus was observed in between 0.1 - 0.22 $m.s^{-1}$ and 0.34 - 0.36 $m.s^{-1}$, where B_{vel} was slightly less than 1 and is not statistically significant at 95%

confidence interval. In addition, a low percentage probability was observed in the following current velocities ranges: 0.38 - 0.5 $m.s^{-1}$ and 0 - 0.06 $m.s^{-1}$.

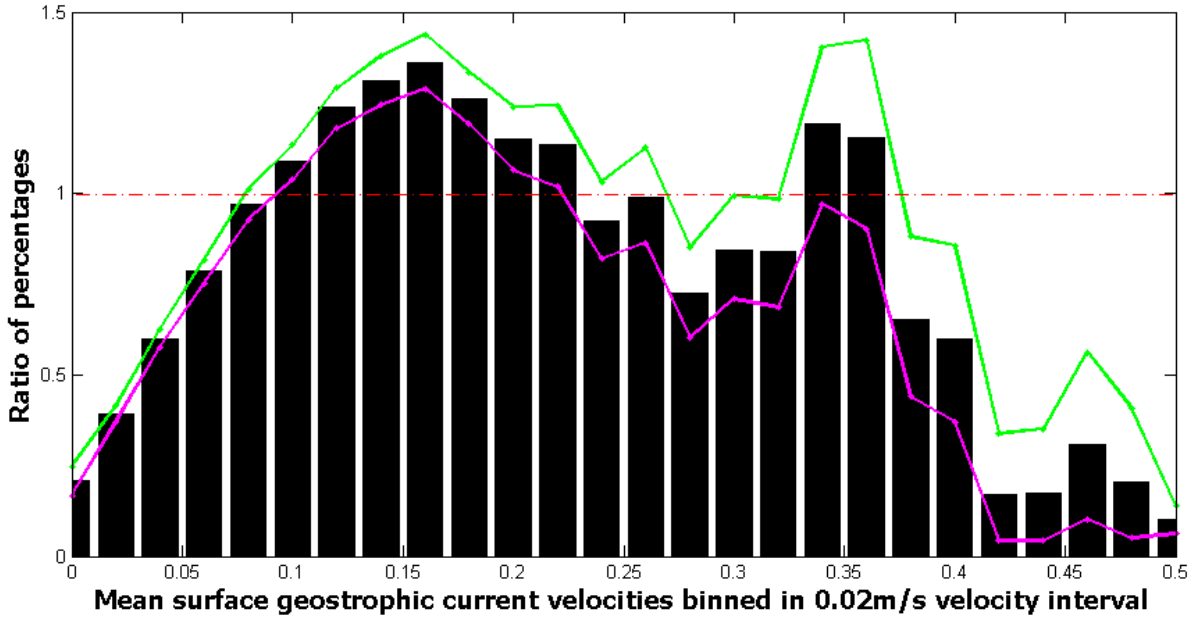

Figure 10: The ratio of the percentages of the co-located Argo profiling floats instances (vel_{floats}) in relation to the surface velocity (as depicted in Figure 8) and the distribution of the mean surface velocity (vel_{total}) (as depicted in Figure 9) of the Southern Ocean south of Africa. This ratio, $B_{vel,}$ provides a quantitative evaluation of the expected presence of floats within certain velocity bins normalized by the velocity distribution present in the region of study. A bias is identified where the ratio, $B_{vel} > 1$ and is statistically significant when the limits of 95 % confidence interval lie above 1.The green and the magenta lines represent the lower and the upper (2.5 % and 97.5 %) limits of the confidence interval respectively.

Figure 11 highlighted the spatial distribution of Argo profiling floats found in regions where the velocities ranged from 0.1 - 0.22 $m.s^{-1}$ (in yellow). The 0.1 - 0.22 $m.s^{-1}$ velocity range was overlaid on to the mean surface geostrophic velocities (Figure 11) to illustrate the spatial distribution of bias of the Argo floats identified in Figure 10. This supports the previous suggestion that the floats aggregated and entrained into higher velocity regions associated with front cores.

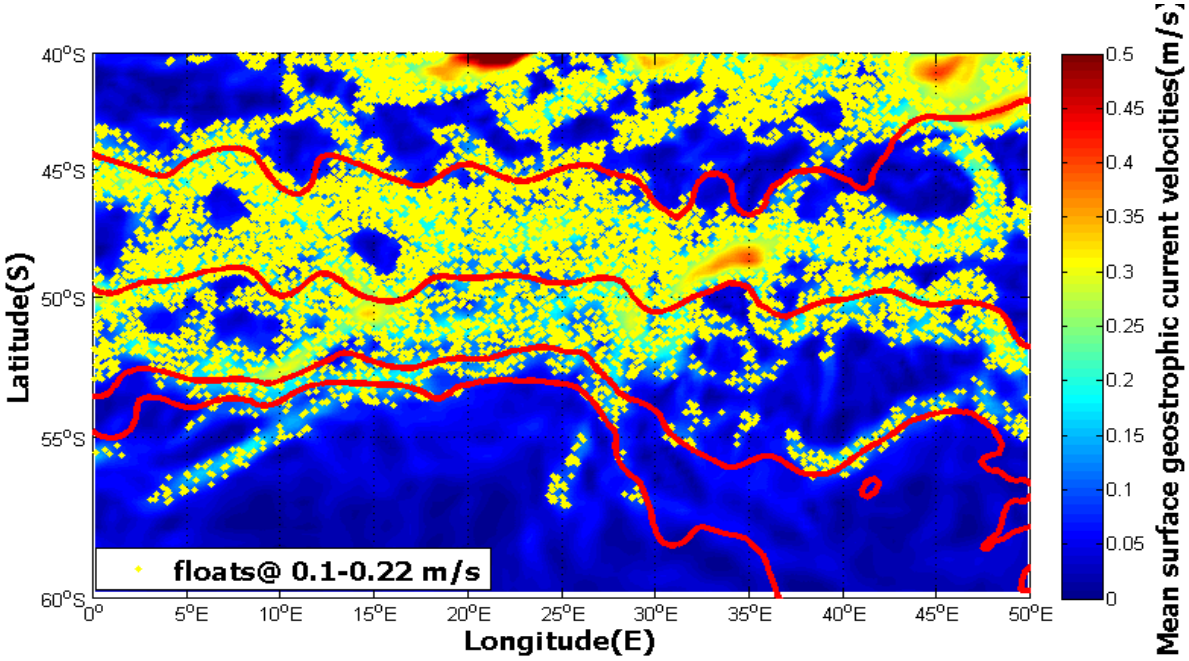

Figure 11: Locations of floats that have positive bias in the velocity bins between 0.1- 0.22 $m.s^{-1}$ (yellow dots) as depicted in Figure 10. The floats are overlaid on to the mean surface geostrophic velocities. The red contours describe the mean location of the main ACC fronts from north to south: SAF, PF, sACCf and SBdy.

4. Discussion

In this section, we discuss the spatial distribution of Argo profiling floats in relation to the bathymetry and the mean surface geostrophic current velocities and whether the results suggest that the spatial distribution of the floats was influenced by the bathymetry or by the surface geostrophic velocities in the Southern Ocean.

4.1. Argo floats and relation to bathymetry

The co-location of floats with the regional bathymetry ($topo_{floats}$) indicated that Argo floats were not uniformly distributed in relation to the entire regional bathymetry ($topo_{total}$) (Figure 3). More floats were found between 4000 - 5400 m depth than at depths shallower than 3500 m. In our study region, 65 % of the total area contained depths deeper than 3500 m. Heezen et al. (1972) explain that the bathymetry of the Southern Ocean south of Africa has three major basins: the Weddell Basin, the Agulhas Basin and the Cape Basin. Of the total floats, 20 % or 33 out of 167 floats were located in the 2400 - 3600 m depth range, which represented 21.6 % of the total ocean area in our focus region, and was dominated by ridges and rises — namely the Southwestern Indian Ridge, Meteor Rise and Conrad Rise (Heezen et al., 1972). Only 3.3 % or 6 out of 167 floats were found in the 0 - 2000 m depth range. This was because floats seldom flowed over shallow topography but rather, they tended to flow around the shallow features that were barriers to the flow of the ACC (Graham et al., 2012). In the 0 - 2000 m depth range it is common to find sea-mounts, plateaus and islands (Figure 6). Although there were fewer shallow depths than deep depths, the former influenced the spatial distribution of the Argo profiling floats.

Argo float trajectories were seen to be influenced by the Agulhas fracture zone (Figure 6), which steered the floats towards the equator to conserve potential vorticity (Gille, 2003). As a result, the floats moved along constant H/f contours, where H is the ocean depth and f is the Coriolis parameter. However, sills (gaps) in the Agulhas fracture zone allowed the Argo floats to move from one ocean basin to another with the deep currents flowing through these gaps. These allow for the transport of heat and the mixing between water masses from Sub-Tropical Zones (STZ) and those of the Sub-Antarctic Zones (SAZ) (Whitworth and Nowlin, 1987). Similarly, Argo float trajectories were deflected northwards towards the equator when approaching the Meteor Rise (47.5° S, 7.5° E) (Figure 6). The Meteor Rise created major perturbations in the trajectories of the floats downstream (Figure 6), where the SAF and PF exhibited wave-like patterns downstream into the Agulhas Basin.

The Southwestern Indian Ridge (SWIR) served as an obstacle to the predominantly zonal flow in the Southern Ocean. The Argo float trajectories were deflected northward and southward in the surroundings of the SWIR. This was because ACC fronts, which are deep reaching (Rintoul et al., 2001; Sokolov and Rintoul, 2007; Sokolov and Rintoul, 2009b), are steered and diverted by the ocean topography to conserve potential vorticity (Graham et al., 2012). As the depth decreases, due to the presence of a shallow topographic barrier, the relative vorticity and Coriolis parameter must also decrease so that potential vorticity was conserved. Pollard and Read (2001) made similar observations of the fragmentation of ACC fronts in the vicinity of SWIR. They explain that these fragmentations of the ACC resulted in several branches of the current as it crossed the SWIR. Moreover, the shear stress from the SWIR led to the convergence of the trajectories of the Argo floats in the vicinity of SWIR. It could be inferred that those converging

zones (north-east sector of Figure 6) marked the positions of the two main branches of the SAF. However, one of the branches turned south or southeast to merge with the PF. Together, they formed the Ob' Lena current (Whitworth and Nowlin, 1987). The Ob' Lena current was located between the Conrad Rise and Crozet Islands.

To the north of the Conrad Rise (50 - 51° S, 40° E), trajectories of Argo floats were trapped between the Conrad Rise and the Crozet Islands (Figure 6). This was due to a fast flowing permanent feature, evident when Argo floats were overlaid onto the altimetry-derived surface geostrophic current velocities (Section 3.2). The Conrad Rise served as another major barrier in the flow of the ACC. The trajectories of Argo floats did not cross the Conrad Rise but rather were deflected north and south of it. Durgadoo et al. (2008) observed similar concentrations of surface drifters to the north and south of the Conrad Rise. Some floats converged south of the Conrad Rise in the Enderby Basin (part of the Weddell Basin). The trajectories of Argo floats in the Enderby Basin suggested that there was a transport of heat to higher latitudes and the presence of a deep cyclonic re-circulation.

In summary, the underlying bathymetry features were shown to influence the distribution of Argo floats and their trajectories in agreement with existing literature on the deep ocean currents in the Southern Ocean. These results showed that the concentration of Argo floats was higher in the deeper ocean basins and lower in the shallower areas. This was particularly evident in Figure 5, which showed that floats were skewed towards deeper ocean depths (4000 - 5000 m). Moreover, there was a higher percentage probability (10 - 30 %) of Argo profiling floats

sampling this region more frequently and was significant at 95 % confidence interval. The floats are more randomly distributed in the 2000 - 3000 m depth range (Figure 5).

4.2. Argo floats and relation to altimetry-derived surface geostrophic current velocities

Argo profiling float positions formed clusters, and when overlaid on to the geostrophic currents, it was evident that their distribution formed banded patterns centered predominantly in the latitudinal zones of SAF and PF. This suggested that floats were regularly entrained into the fronts of the ACC. Hofman (1985) observed similar continuous patterns of high buoy density across the Atlantic sector of the Southern Ocean. South of Africa, Hofman (1985) observed that there were isolated areas of high buoy density, and she concluded that surface drifters have a preference for flowing in or near the frontal zones of the ACC.

It was evident from Figure 11 that ocean currents influenced the distribution of Argo profiling floats. Particularly, in this case, the banded patterns of the Argo floats were located more in zones with higher mean surface geostrophic velocities (0.1 - 0.22 $m.s^{-1}$) and were statistically significant at 95 % confidence interval. Sokolov and Rintoul (2007, 2009a and 2009b) explain that the ACC fronts are deep reaching (> 2000 m). Consequently, floats became entrained in the frontal zones by convectional mechanisms such as Ekman pumping. As floats ascended to the surface, they ended up being entrained in the Ekman layers. The Ekman layers converged and diverged in response to wind stress. The convergence of the Ekman layers led to the entrainment of floats into regions of higher surface velocities. Furthermore, the convergence of the Ekman layers led to an increase in sea surface heights. Constant dynamic heights could be used to mark

the latitudinal position of the ACC fronts (as done in Sokolov and Rintoul, 2009b and Swart et al., 2008; 2010).

The results suggested that there was up to a 40 % higher probability of finding Argo floats where current velocities ranged from 0.1 - 0.22 $m.s^{-1}$ (Figure 10) and this velocity range was statistically significant at 95 % confidence interval. This indicated that floats were entrained into frontal regions and preferentially sampled regions where the ocean current velocities were higher. The bias found in 0.34 - 0.36 $m.s^{-1}$ was not statistically significant at 95 % confidence interval, although there was a 20 - 25 % higher probability of finding Argo floats in that interval.

5. Summary and challenges

Surface drifters have provided the scientific community with the knowledge necessary in understanding the nature and dynamics of the ACC. Hofman (1985) examined both the circumpolar nature and the surface structure of the ACC based on the distribution density of the surface drifters (buoys). The buoys accumulated in latitudinal zones of the SAF and the PF. In addition, Durgadoo et al. (2008) used surface drifters together with altimetry and stimulated velocities from model to investigate the flow of the ACC around the Conrad Rise. They explained that the ACC bifurcated as it approached the Conrad Rise. As a result, two intense jets were formed north and south of the Conrad Rise (Durgadoo et al., 2008). Although surface drifters had contributed to understanding the surface structure of the ACC and in determining the mean surface velocities of ACC fronts, Argo floats provided the opportunity to sample continuously and persistently the deep ocean state of the Southern Ocean and the large scale subsurface ocean variability (Roemmich and Gilson, 2009). Argo floats also removed the constraint of needing to have research vessels present at the time of measurement and were comparatively cheap. These floats made it possible to obtain high quality data from remote regions regularly and in near real time.

In this study, we investigated the spatial distribution of Argo floats in the Southern Ocean south of Africa and its relation to the underlying bathymetry and the geostrophic currents. The results highlighted the effects of the underlying topography on the ACC as well as the horizontal structure of the ACC, comparing Argo float positions to mean geostrophic currents. The study showed that trajectories of the Argo floats were influenced by the topographic steering of the

ACC by the underlying bathymetry, related to the conservation of potential vorticity. In agreement with previous literature, it was shown that the deep currents containing the Argo floats could not flow across shallow bathymetric features. This led to an increase in the concentration or convergence of floats in 4000 - 5000 m depth range. Furthermore, bias at this aforementioned depth was significant at 95 % confidence interval. The trajectories of Argo floats also illustrated that there was a clockwise re-circulation in the Weddell Basin. In addition, the convergence of floats suggested that they became entrained into the fronts of the ACC as conceptually depicted in Figure 12.

By mapping the deep reaching currents of the ACC using the trajectories of Argo floats, it was observed that floats were entrained into regions with higher mean surface geostrophic current velocities. The floats formed banded patterns at latitudes associated with the SAF and the PF, which was evident when floats were overlaid on to the mean geostrophic currents. The float distributions were also preferentially found in the permanent Ob' Lena current between the Crozet Islands and Conrad Rise (Whitworth and Nowlin, 1987). In addition, the study highlighted an important link between the deep reaching fronts of the ACC fronts and the surface geostrophic current patterns, confirming that the fronts were consistently deep reaching.

Although Argo floats have revolutionized the study of the ocean, this study highlighted that the lagrangian floats do not uniformly sample the Southern Ocean. This was because they aggregated in frontal zones (as depicted in Figure 12). Therefore, spatial biases, which are significant at 95 % confidence interval, could be introduced when these data were used to

generate gridded data and climatology to characterize the oceanography or understand the distribution and variability of oceanographic processes and their relation to climate. Alternative technologies currently available or under development may be able to overcome this problem through adaptive sampling and remote control, such as ocean gliders and other piloted, semi-autonomous platforms (Roemmich and Gilson, 2009).

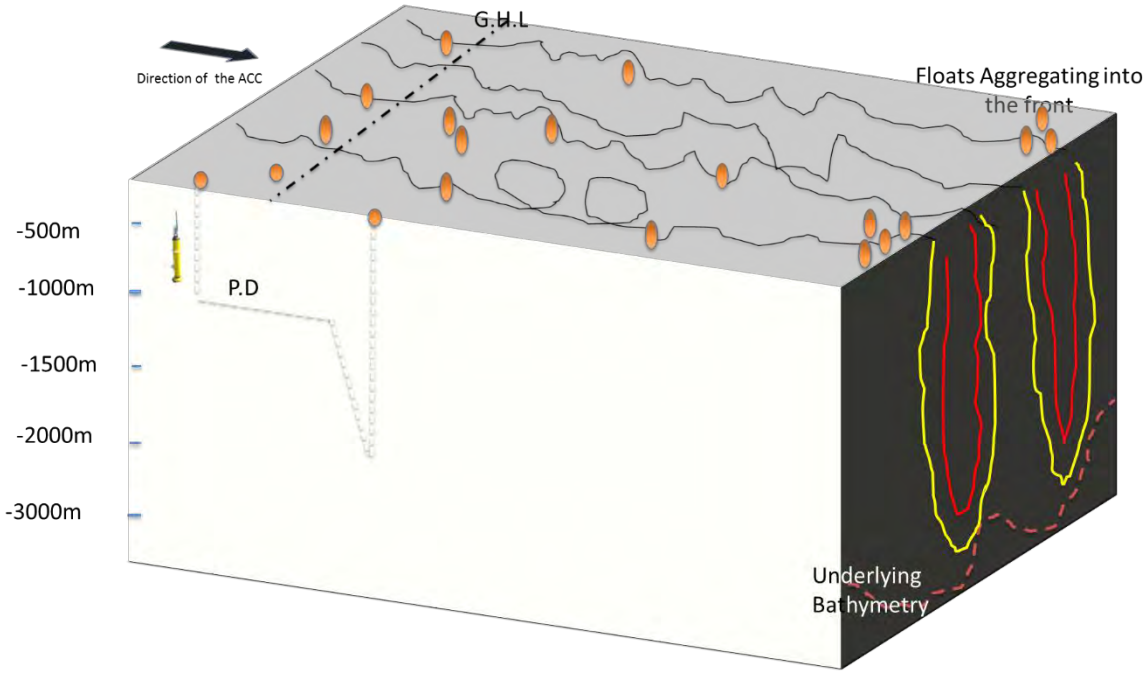

Figure 12: A conceptual diagram describing the Argo floats sampling sequence and the deep reaching fronts of the ACC. The Argo floats drift for 10 days at the parking depth (PD). The floats at the GoodHope Line (GHL) are normally distributed evenly in uniform fashion. Downstream, these floats aggregate as they are entrained into the fronts after deployment. The cores of the fronts are seen to be deep reaching and therefore are impacted by underlying topography resulting in meandering and spatial variability in the distribution of the fronts.

ACKNOWLEDGEMENTS

I would like to thank my supervisors Sebastian Swart and Björn Backeberg for facilitating the smooth running of this project. Without their expertise I would never have had access to or understood materials necessary for this research. I would like to thank the AMS class of 2014 for their friendship and support. I am deeply grateful to Marcel du Plessis and Louis du Buisson for helping me with MATLAB. In addition, I would like to thank Coleen Moloney for her mentorship.

I am grateful and appreciate the financial supports from National Research foundation (NRF), University of Cape Town's Marine Research Institute (Ma-Re), Partnership for the Observations of the Global Ocean (POGO), Nansen-Tutu Centre for Marine Environment Research and the Applied Centre for Earth System Science (ACCESS). A final thanks to the Almighty God and my mum for supporting me throughout my studies at UCT.

Plagiarism Declaration

I know the meaning of plagiarism and declare that all of the work in this dissertation, excluding that which is properly acknowledged, is my own.

References

Ansorge, I.J., Speich, S., Lutjeharms, J.R.E., Goni, G.J., Rautenbach, C.J., Froneman, W., Rouault, M. and Garzoli, S. (2004). Monitoring the oceanic flow between Africa and Antarctica. *South African Journal of Science*, 101, 29 - 35

Argo (2000). Argo float data and metadata from Global Data Assembly Centre (Argo GDAC). Ifremer.doi.org/10.12770/1282383d-9b35-4eaa-a9d6-4b0c24c0cfc9

Belkin, I.M. and Gordon, A.L. (1996). Southern Ocean fronts from the Greenwich meridian to Tasmania. *Journal of Geophysical Research*, 101, 3675 - 3696

Bryden, H.L., Beal, L.B. and Duncan, L.M. (2005). Structure and transport of the Agulhas Current and its temporal variability. *Journal of Oceanography*, 61, 479 - 492

Deacon, G.E.R. (1937). The hydrology of the Southern Ocean. *Discovery*, 15, 1 - 124

Durgadoo, J.V., Lutjeharms, J.R.E., Biastoch, A. and Ansorge, I.J. (2008). The Conrad Rise as an obstruction to the Antarctic Circumpolar Current. *Geophysical Research Letters*, 35, L20606.doi:10.1029/2008GL035382

Gille, S.T. (2003). Float observations of the Southern Ocean: Part 1, Estimating mean fields, bottom velocities, and topographic steering. *Journal of Physical Oceanography*, 33, 1167 - 1181

Gille, S.T. (2008). Decadal-scale temperature trends in the southern hemisphere ocean. *Journal of Climate* 21: 4,749 - 4,765

Gille, S.T. and Kelly, K.A. (1996). Scales of spatial and temporal variability in the Southern Ocean. *Journal of Geophysical Research*, 101, 8759 - 8774

Gladyshev, S., Arhan, M., Sokov, A. and Speich, S. (2008). A hydrographic section from South Africa to the southern limit of the Antarctic Circumpolar Current at the Greenwich meridian. *Deep-Sea Research,* Part I, 55, 1284 - 1303.doi:10.1016/j.dsr.2008.05.009

Gordon, A.L. (1986). Inter - ocean exchange of thermocline water. *Journal of Geophysical Research,* 91, 5037 - 5046

Graham, R.M., de Boer, A.M., Heywood, K.J., Chapman, M.R. and Stevens, D.P. (2012). Southern Ocean fronts: controlled by wind or topography? *Journal of Geophysical Research*, 117, C08018.doi:10.1029/2012JC007887

Heezen, B.C., Tharp, M. and Bentley, C. (1972). Morphology of the earth in the Antarctic and Sub-Antarctic. *American Geography Society*

Hofmann , E.E. (1985). Large-scale horizontal structure of the Antarctic Circumpolar Current. *Journal of Geophysical Research,* 90, 7087 - 7097

Le Traon, P.Y., Dibarboure, G. and Ducet, N. (2001). Use of a high resolution model to analyze the mapping capabilities of multiple-altimeter missions. *Journal of Atmospheric and Oceanic Technology*, 18, 1277 - 1288

Le Traon, P.Y., Nadal, P.F. and Ducet, N. (1998). An improved mapping method of multi-satellite altimeter data. *Journal of Atmospheric and Oceanic Technology*, 15, 522 - 534

Lombard, A., Cazenave, A., Le Traon, P.Y. and Ishii, M. (2005). Contribution of thermal expansion to present-day sea level change revisited. *Global Planet Change*, 47, 1 - 16. doi:10.1016/j.gloplacha.2004.11.016

Lutjeharms, J. (2006). *The Agulhas Current*. Springer, Berlin

Moore, J.K., Abbott, M.R. and Richman, J.G. (1999). Location and dynamics of the Antarctic Polar Front from satellite sea surface temperature data. *Journal of Geophysical Research*, 104, 3059 - 3073.doi:10.1029/ 1998JC900032

Morrow, R., Valladeau, G. and Salle, J.B. (2008). Observed subsurface signature of Southern Ocean sea level rise. *Progress in Oceanography,* 77, 351 - 366. doi:10.1016/j.pocean.2007.03.002

National Geophysical Data Center/NESDIS/NOAA/U.S. Department of Commerce. (2001). ETOPO2, Global 2 Arc-minute Ocean Depth and Land Elevation from the US National Geophysical Data Center (NGDC). Research Data Archive at the National Center for Atmospheric Research, Computational and Information Systems Laboratory, Boulder, CO.doi.org/10.5065/D6668B75

Nowlin, W.D. and Clifford, M. (1982). The kinematic and thermo-haline zonation of the Antarctic Circumpolar Current at Drake Passage. *Journal of Marine Research,* 40, 481-507

Ollitraut, M. and Rannou , J.P. (2012). ANDRO: An Argo-based deep displacement dataset. *American Meteorological Society.*doi: 10.1175/jtech-d-12-00073.1

Orsi, H., Whitworth, T. and Nowlin, W.D.Jr. (1995). On the meridional extent and fronts of the Antarctic Circumpolar Current. *Deep-Sea Research*, Part I, 42, 641-673. doi:10.1016/0967-0637 (95)00021-W

Park, Y.H., Charriaud, E. and Craneguy, P. (2001). Fronts, transport, and Weddell Gyre at 30º E between Africa and Antarctica. *Journal of Geophysical Research,* 106, 2857 - 2879

Pollard, R.T. and Read, J.F. (2001). Circulation pathways and transports of the Southern Ocean in the vicinity of the Southwest Indian Ridge. *Journal of Geophysical Research*, 106, 2881 - 2898

Rintoul, S.R., Hughes, C. and Olbers, D. (2001). The Antarctic Circumpolar Current system, in *Ocean Circulation and Climate*, edited by Siedler, G., Church, J.A. and Gould, J. Elsevier, New York

Rio, M.H., Guinehut, S. and Larnicol, G. (2011). New CNES-CLS09 global mean dynamic topography computed from the combination of GRACE data, altimetry, and in situ measurements. *Journal of Geophysical Research*, 116, C07018.doi:10.1029/2010JC006505

Roemmich, D. and Gilson, J. (2009). The 2004 - 2007 mean and annual cycles of temperature, salinity and steric height in the global ocean from the Argo Program. *Progress in Oceanography*.doi:10.1016/ j.pocean.2009.03.004

Sandwell, D.T. (1990). Geophysical applications of satellite altimetry. *Reviews of Geophysics Supplement*, 132 - 137

Sandwell, D.T. and Smith, W.H.F. (1997). Global sea floor topography from satellite altimetry and ship depth soundings. *Journal of Geophysical Research,* 102, 10039

Sandwell, D.T. and Zhang, B. (1989). Global mesoscale varability from geosat exact repeat mission: correlation with ocean depth. *Journal of Geophysical Research,* 94, 17, 971 - 17, 984

Sievers, H.A. and Nowlin, W.D.Jr. (1984). The stratification and water masses at Drake Passage. *Journal of Geophysical Research*, 89, 10 489 - 10 514

Sokolov, S. and Rintoul, S.R. (2002). Structure of Southern Ocean fronts at 140º E. *Journal of Marine Systems*, 37, 151 - 184.doi:10.1016/S0924-7963(02)00200-2

Sokolov, S. and Rintoul, S.R. (2007). Multiple jets of the Antarctic Circumpolar Current south of Australia. *Journal of Physical Oceanography,* 37, 1394 - 1412.doi:10.1175/JPO3111.1

Sokolov, S. and Rintoul, S.R. (2009a). Circumpolar structure and distribution of the Antarctic Circumpolar Current fronts: 1. Mean circumpolar paths. *Journal of Geophysical Research*, 114, C11018.doi:10.1029/2008JC005108

Sokolov, S. and Rintoul, S.R. (2009b). Circumpolar structure and distribution of the Antarctic Circumpolar Current fronts: 2. Variability and relationship to sea surface height. *Journal of Geophysical Research*, 114, C11019.doi:10.1029/2008JC005248

Swart, S., Speich, S., Ansorge, I.J., Goni, G.J., Gladyshev, S. and Lutjeharms, J.R.E. (2008). Transport and variability of the Antarctic Circumpolar Current south of Africa. *Journal of Geophysical Research*, 113, C09014.doi:10.1029/2007JC004223

Swart, S., Speich, S., Ansorge, I.J. and Lutjeharms, J.R.E. (2010). An altimetry-based gravest empirical mode south of Africa:1.Development and validation. *Journal of Geophysical Research.*doi:10.1029/2009JC005299, in press

Talley, L.D., Pickard, G.L., Emery, W.J. and Swift, H.J. (2011). *Descriptive Physical oceanography.*6th Ed. Elsevier, Oxford

Whitworth, T. and Nowlin, W.D.Jr. (1987). Water masses and currents of the southern ocean at the Greenwich Meridian. *Journal of Geophysical Research,* 92, 6462 - 6476. doi:10.1029/JC092iC06p06462

Willis, J.K., Roemmich, D. and Cornuelle, B. (2004). Inter-annual variability in upper-ocean heat content, temperature and thermo-steric expansion on global scales. *Journal of Geophysical Research*. 109, C12036. doi:10.1029/2003JC002260